Self-stacked 1T-1H layers in 6R-NbSeTe and the emergence of charge and magnetic correlations due to ligand disorder

S. K. Mahatha,[1,2,*] J. Phillips,[3,4,*] J. Corral-Sertal,[3,5,*] D. Subires,[6] A. Korshsunov,[7] A. Kar,[6] J. Buck,[2,8] F. Diekmann,[2,8] G. Garbarino,[9] Y. P. Ivanov,[10] A. Chuvilin,[11,12] D. Mondal,[13,14] I. Vobornik,[13] A. Bosak,[7] K. Rossnagel,[2,15] V. Pardo,[3,4] Adolfo O. Fumega,[16] and S. Blanco-Canosa[6,12,†]

[1] *UGC-DAE Consortium for Scientific Research, University Campus, Khandwa Road, Indore-452001, India*
[2] *Ruprecht Haensel Laboratory, Deutsches Elektronen-Synchrotron DESY, 22607 Hamburg, Germany*
[3] *Departamento de Física Aplicada, Universidade de Santiago de Compostela, E-15782 Campus Sur s/n, Santiago de Compostela, Spain*
[4] *Instituto de Materiais iMATUS, Universidade de Santiago de Compostela, E-15782 Campus Sur s/n, Santiago de Compostela, Spain*
[5] *CiQUS, Centro Singular de Investigacion en Quimica Biolóxica e Materiais Moleculares, Departamento de Quimica-Fisica, Universidade de Santiago de Compostela, Santiago de Compostela, E-15782, Spain.*
[6] *Donostia International Physics Center (DIPC), San Sebastián, Spain*
[7] *European Synchrotron Radiation Facility (ESRF), BP 220, F-38043 Grenoble Cedex, France*
[8] *Institut für Experimentelle und Angewandte Physik, Christian-Albrechts-Universität zu Kiel, D-24098 Kiel, Germany*
[9] *European Synchrotron Radiation Facility (ESRF), BP 220, F-38043 Grenoble Cedex 9, France*
[10] *Electron Spectroscopy and Nanoscopy, Istituto Italiano di Tecnologia, Via Morego 30, 16163 Genova, Italy*
[11] *CIC Nanogune, San Sebastián, Spain*
[12] *IKERBASQUE, Basque Foundation for Science, 48013 Bilbao, Spain*
[13] *Consiglio Nazionale delle Ricerche (CNR)- Istituto Officina dei Materiali (IOM), Laboratorio TASC in Area Science, Trieste, Italy*
[14] *Sovarani Memorial College, Jagatballavpur, Howrah - 711408, India*
[15] *Institut für Experimentelle und Angewandte Physik, Christian-Albrechts-Universität zu Kiel, 24098 Kiel, Germany*
[16] *Department of Applied Physics, Aalto University, 02150 Espoo, Finland*

(Dated: May 2024)

The emergence of correlated phenomena arising from the combination of 1T and 1H van der Waals layers is the focus of intense research. Here, we synthesize a self-stacked 6R phase in NbSeTe, showing a perfect alternating 1T and 1H layers that grow coherently along the c-direction, as revealed by scanning transmission electron microscopy. Angle-resolved photoemission spectroscopy shows a mixed contribution of the trigonal and octahedral Nb bands to the Fermi level. Diffuse scattering reveals temperature-independent short-range charge fluctuations with propagation vector q_{CO}=(0.25,0), derived from the condensation of a longitudinal mode in the 1T layer, while the long-range charge density wave is quenched by ligand disorder. Magnetization measurements suggest the presence of an inhomogeneous, short-range magnetic order, further supported by the absence of a clear phase transition in the specific heat. These experimental analyses in combination with *ab initio* calculations indicate that the ground state of 6R-NbSeTe is described by a statistical distribution of short-range charge-modulated and spin-correlated regions driven by ligand disorder. Our results devise a route to synthesize 1T-1H self-stacked bulk heterostructures to study emergent phases of matter.

I. INTRODUCTION

Layered van der Waals (vdW) materials consisting of the stacking of two-dimensional (2D) transition metal dichalcogenide (TMD) layers offer a fertile playground to realize novel physical phenomena [1–3]. The great versatility of the TMD's chemical structure and the presence of a vdW gap allows the intercalation of a large variety of atomic species, offering endless possibilities for materials engineering [4], emergence of correlated phases or tuning the balance between different competing orders that intertwine with the ground state of the vdW layers [5–12].

The most common strategy to engineer vdW heterostructures is a bottom-up approach where single layers are exfoliated and stacked together forming few-layer slabs [13, 14]. This approach takes advantage of the unique degrees of freedom encountered in vdW materials, such as the twist angle between layers or the combination of layers with different symmetry-breaking orders to design and tune strongly correlated electronic phases [15–21].

Nevertheless, in bulk TMDs, the growth and stacking of different layers turns out to be experimentally demanding, and limited to the metastable $4H_b$ phase of TaS_2 [22]. This vdW heterostructure benefits from the stacking of the strongly correlated insulating 1T layers,

* These authors contributed equally to this work.
† sblanco@dipc.org

featuring nearly flat bands [23], and the metallic 1H layer to promote chiral superconductivity and topological edge modes [24, 25]. A similar 6R-phase, stacking 1T-1H layers of TaS_2 hosting a charge density wave (CDW), becomes superconducting with higher T_c than the parent compound [26]. Therefore, achieving an alternating 1T-1H bulk heterostructure in systems other than TaS_2 would expand the possibilities to explore the complex phase diagram of correlated phases in TMDs.

Here, we present an alternative route to obtain 1T-1H bulk structures, and in particular the 6R-phase of NbSeTe. This kind of heterostructure can be synthesized by the chemical substitution of the chalcogen atom (S, Se, or Te) from the parent 1T-$NbTe_2$ and 2H-$NbSe_2$ bulk phases. The chemical ligand-doping of the parent compounds opens the possibility of tuning lattice symmetries and artificially creating new electronic ground states. For instance, the distorted quasi-1D 1T structure of $NbTe_2$ is characterized by a first-order-like CDW transition [27], while the 2H polytype of $NbSe_2$ develops at low temperature a superconducting ground state coexisting with CDW order [28–30]. Monolayer $NbSe_2$ has also been predicted to present strain and impurity dependent CDW configurations associated to a 4×4 modulation [31, 32]. Given the extreme versatility of the vdW TMD fabric and the proximity of collective phenomena with similar energy scales, the random substitution of the TMD ligand offers new avenues to engineer novel ground states and the possibility of targeted functionalities. For instance, recently, the metastable layered compound 1T-NbSeTe has been synthesized [33], highlighting the first pure 1T superconducting phase within the TMD family. Furthermore, the chemical substitution of Te by Se in the solid solution $TaSe_{2-x}Te_x$ (already superconducting in bulk form [34, 35]) has been predicted to give rise to emergent phases and topological superconductivity at the monolayer limit [36].

In this work, we tweak the growth parameters to chemically combine 2H-$NbSe_2$ and 1T-$NbTe_2$ producing a 6R-phase of bulk NbSeTe, described by a perfect 3×stacking of c-axis oriented 1T−1H heterobilayers. This rhombohedral 6R structure shows a decoupling of the vdW layers that weakens the charge correlations of the parent compounds and allows the emergence of a glassy-type short-range competing magnetic order. Remarkably, the short-range charge correlations appear as diffuse scattering with in-plane propagation vector q_{CO}=(0.25,0) and are driven by the condensation of a phonon of the 1T-Nb layer that strongly competes with a different charge modulation with propagation vector $\left(q^* = \frac{1}{6}, \frac{1}{6}\right)$ in the same 1T-Nb slab. *Ab initio* calculations show that this kind of charge ordering emerges independently of the in-plane Se/Te disorder pattern and presumably introduces local strains that drive local magnetic order. Our work describes a path to study hidden phases and demonstrates that the large versatility of the layered TMD structure allows tuning the structural, magnetic, and electronic properties to reveal hidden phases of matter.

II. RESULTS

Let us start by analyzing in detail the 6R structure of NbSeTe. Figure 1(a) demonstrates the coherent layered growth of NbSeTe. Further, atomic resolution annular dark-field in the scanning transmission electron microscope (ADF-STEM) imaging, Fig. 1(e) and (f), shows a perfect stacking of 1T and 1H layers, where we can identify and assign the Nb atoms sandwiched between the chalcogen layers that feature both a trigonal, 1H, and octahedral, 1T, coordination. The conventional unit cell of the 6R-NbSeTe structure is shown in Figs. 1(c) and 1(g). The high-resolution transmission electron microscopy (TEM) also resolves an in-plane shift of consecutive bilayers of ($\frac{1}{3}$, -$\frac{1}{3}$) (Fig. 1(f)) in the unit cell defined in Fig. 1 (c), being the overall structure described by a rhombohedral primitive unit cell with space-group symmetry *R3m* (no. 160). The alternating 3× 1T-1H consecutive heterobilayers, Fig. 1(g), is confirmed by x-ray diffraction (Supplementary Information, Fig. S4) that provides the lattice parameters a=b= 3.53 Å and c= 39.26 Å, for a Se/Te ratio of 0.91, as obtained from energy dispersive analysis (EDX). Results of core level x-ray photoelectron spectroscopy (XPS) measurements are shown in Fig. 1(b), presenting data obtained with an incident photon energy E_{in}= 333 eV. It shows the emissions from the spin-orbit split bands of $3d$ ($4d$) orbitals of Nb and Se (Te) at 220 and 55 (40) eV below the Fermi level, respectively. Besides, the $3p$ emissions are also observed at 160-166 eV, in good agreement with the XPS spectra of $NbSe_2$ and $NbTe_2$ and reports in the literature [37]. Figure 1(h) shows the EDX atomic resolution maps after noise reduction of the structure, which show that Se and Te are stochastically distributed, discarding a Janus-type coherent growth. The disorder between ligands will have a major impact on the emergence of short-range charge and magnetic correlations.

Having structurally characterized the 6R phase of NbSeTe single crystals, we proceed with the study of its electronic structure. Figure 2(a) displays the experimental hexagonal Fermi surface obtained at 447 eV photon energy (see ARPES geometry in Fig. 2 (j)), which can be compared with the Fermi surface calculated using density functional theory (DFT) shown in Fig. 2(b). It consists of two hole-like circular pockets around Γ (mainly with anionic character) and K (of Nb(H) character) and one electron-like "dogbone" centered at M (coming mainly from Nb(H) bands), resembling the 2H-polymorph of $TaSe_2$ [38]. The additional hole pocket centered at Γ, which is absent in 2H-$TaSe_2$, comes from Nb(T) layers (see Supplementary Information, Fig. S5).

We can further analyze the band structure in more detail in an energy region below the Fermi level. The ARPES results are presented in Fig. 2(c-h) along the high symmetry directions together with the corresponding bands (with the main band character denoted by colors) obtained from DFT calculations. Qualitatively, the energy versus wavevector intensity maps match ex-

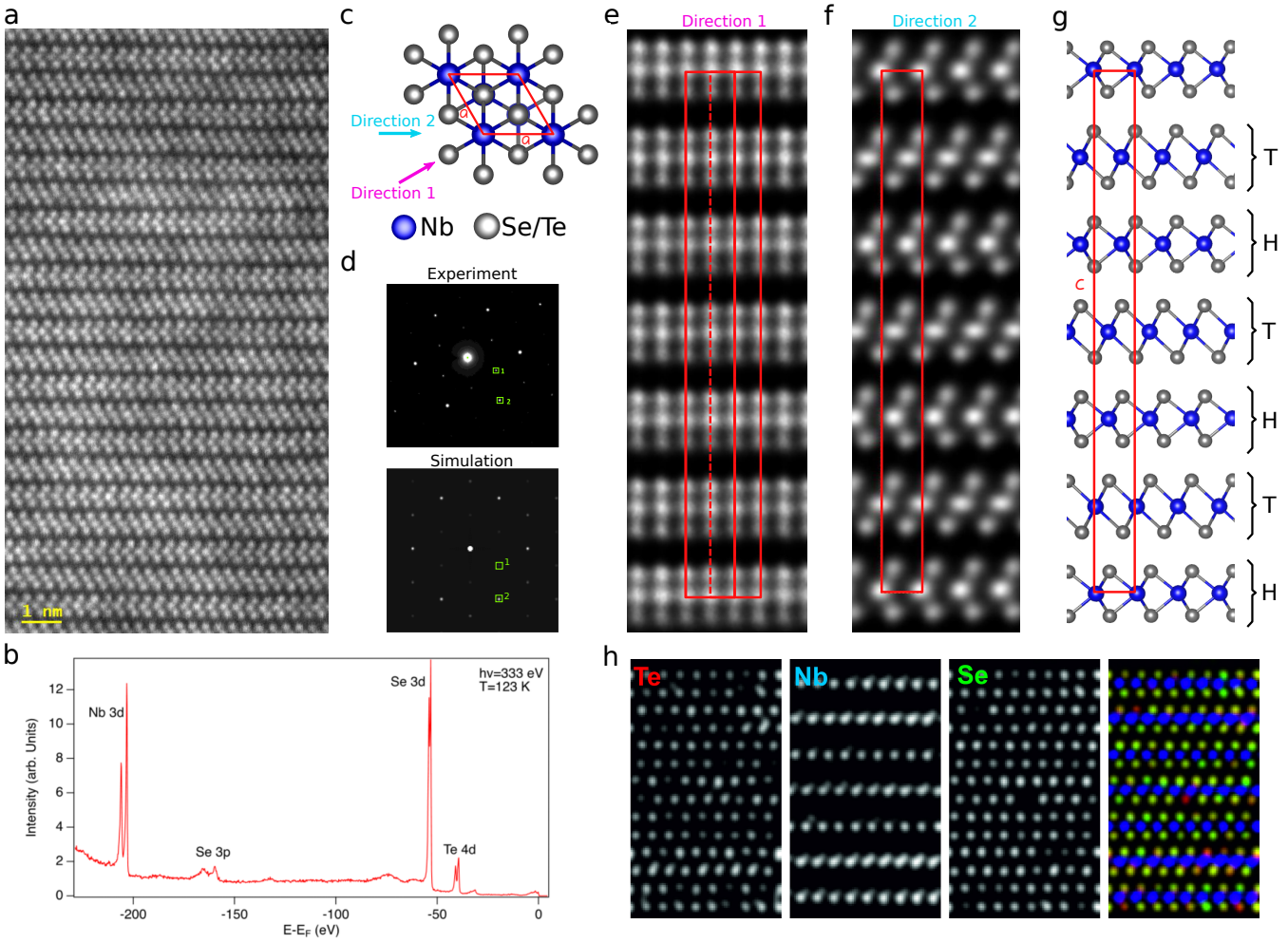

FIG. 1. (a) Large area ADF-STEM image of the sample showing the coherent growth of a layered van der Waals structure. (b) Core level x-ray photoemission, showing the principal emission lines of Nb, Se, and Te. (c) Top view of the 6R-NbSeTe unit cell showing the directions of the ADF-STEM lateral images (e) and (f). (d) Experimental electron diffraction patterns in 6R-NbSeTe in the 001 direction and simulation considering a stochastic distribution of the ligands atoms. (e-f) ADF-STEM lateral images highlighting the 1T-1H heterobilayer in the 6R-NbSeTe. A (1/3,-1/3) in-plane displacement of the 1T-1H bilayer can be seen in (f) and in the lateral view of the conventional unit cell in (g). (h) EDX atomic resolution maps of the image shown in (f) reveal that Se and Te are distributed stochastically (images processed for noise reduction).

tremely well with the simulated bands, both along the Γ-M and Γ-K directions. Our results show no evidence of gap opening at the Fermi level, and Fermi surface nesting appears to be weak at $q_{CDW}=2/3\overline{\Gamma M}$ and $q_{CDW}=2/3\overline{\Gamma K}$ [39]. In Fig. 2(j) we show the calculated density of states in a layer-resolved fashion, showing separately the contribution from Nb d-bands originating from T and H layers. We see that the anion p weight close to the Fermi level is relatively small, although some pieces of the Fermi level do come from anion p orbitals, with a larger Te character close to the Fermi level (the Te p bands will be typically higher in energy than the Se p bands) [36].

We note that the absence of clear translation vectors that may nest portions of the Fermi surface does not preclude the presence of charge modulations. Indeed, this is a common occurrence in TMDs, dominated by electron-phonon interactions for the CDW formation [40–43]. This is illustrated in Fig. 3, where we present the diffuse scattering (DS) data. First, we observe strong diffuse rods of intensity in between Bragg peaks along the L direction, characteristic of a coherent growth of a 2D layered structure, see Fig. 3(b). Second, the diffuse scattering (DS) maps reveal the presence of a diffuse signal, characteristic of a precursor of charge modulations, in the HK0 plane, with in-plane propagation vector $q_{CO}=(0.25\ 0)$ r.l.u. We also notice that the DS develops a sizable intensity in the vicinity of the (1 1 0) Bragg reflection. This DS does not match either the propagation vector of the charge modulations of the bulk 2H-$NbSe_2$ [44] or 1T-$NbTe_2$ [45]. The diffuse clouds in the HK0 plane are

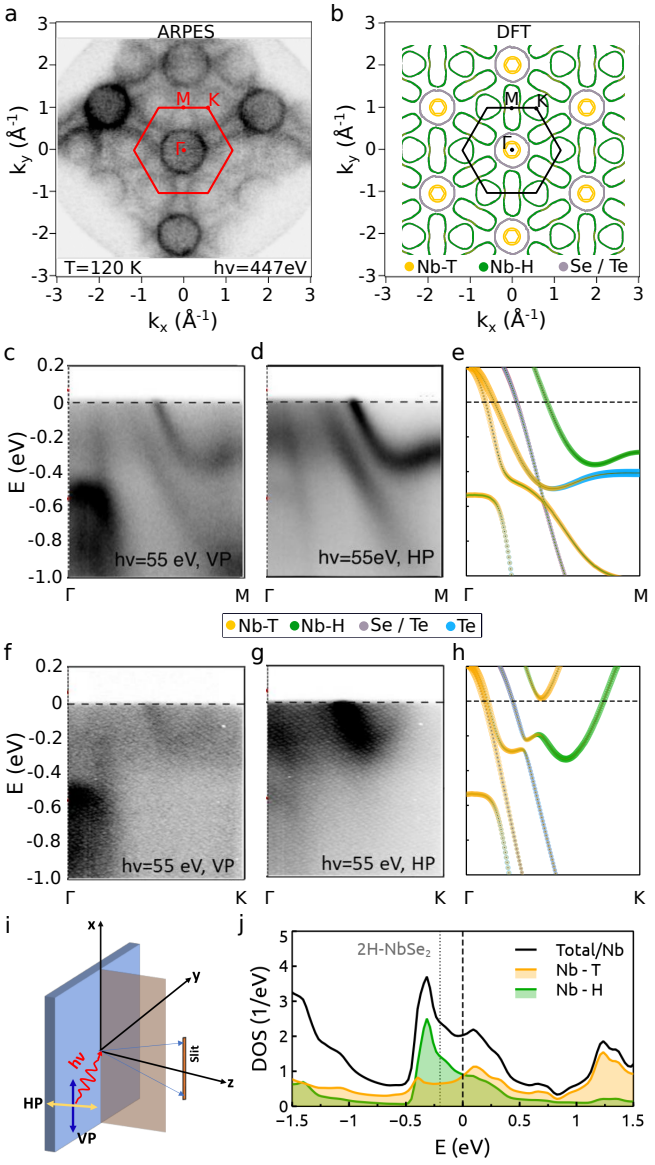

FIG. 2. (a) Fermi surface map of the NbSeTe single crystal at $h\nu$= 447 eV, T= 120 K. (b) Calculated Fermi surfaces using DFT. The different colors indicate the dominant contribution of each sheet in the Fermi surface. (c)-(d) Γ-M normal emission ARPES spectra of NbSeTe and the calculated band structure obtained from DFT (e) for a similar energy interval around the Fermi level and also in the Γ-M direction. (f)-(g) Γ-K Normal emission ARPES spectra of NbSeTe along with DFT calculated band structure (h). The ARPES spectra were obtained with 55 eV incident photon energy with vertical (c)-(f) and horizontal (d)-(g) polarization. (i)ARPES experimental geometry with the linear horizontal polarized (HP) and vertical polarized (VP) light vectors. (j) Calculated density of states showing the contribution from the different Nb atoms in the structure, namely those in T- and H- layers. The dotted vertical line at -0.20 eV shows the location of the Fermi level for 2H-$NbSe_2$ in the projected DOS of Nb-H in 6R-NbSeTe.

indicative of a 0-dimensional structure without an in-plane ordering. The short-range correlation length of the charge fluctuations amounts to 3-4 nm in the a-b plane and does not vary with lowering the temperature down to 80 K, suggesting that the charge correlations are static and do not involve a soft mode. In the H0L plane, the DS is present as diffuse streaks of intensity along the c-axis, Fig. 3(b). The elongated rod in the DS indicates that the signal comes from in-plane atomic displacements perpendicular to the c-direction, hence concentrating the charge fluctuations within a single Nb-TMD layer of the 3×1T-1H heterobilayer.

In order to elucidate the presence of charge correlations in 6R-NbSeTe, we have calculated the phonon dispersion of the ordered 1T(Te)-1H(Se) in the 6R-NbSeTe structure [Fig. 3(c)]. It shows three imaginary soft modes at the propagation vector we observe experimentally; i.e., $q_{CO}=\frac{1}{2}\overline{\Gamma M}$=(0.25, 0) r.l.u. The soft acoustic branches do not share any resemblance with the charge modulations in the parent phases of $NbSe_2$ and $NbTe_2$, which adopt 3×3 CDW ordering at 33 K and 170 K, respectively. Besides, a Fermi surface nesting scenario fails to explain the formation of a CDW in NbSeTe, where the short-range correlations and the absence of temperature dependence of the DS point to the strong coupling mechanisms of the CDW. These triply degenerate soft modes correspond to each of the three 1T-$NbTe_2$ layers of the 6R-NbSeTe heterostructure and describe an in-plane vibration of the Nb atoms. Furthermore, the corresponding Nb atoms of the consecutive 1H-$NbSe_2$ layer appear static; i.e., do not follow the 1T-Nb displacement, hence the 1T-Nb vibration is completely sandwiched between 1H-Nb layers. The lattice dynamics are fully consistent with the observations of the strong DS perpendicular to the HK plane of Fig. 3(b). On the other hand, the phonon calculations also unveil a second instability at q=($\frac{1}{6}$, $\frac{1}{6}$) in the $\Gamma-K$ path describing also the in-plane Nb vibration of the 1T-$NbTe_2$, not observed in the DS experiments. The observation of only one of the instabilities hints at the competition between the two types of charge periodicities, akin to the high-T_c cuprates [46, 47], kagome materials [48–50] or similar TMD van der Waals compounds[42].

To mimic the effect of chemical disorder, we have exchanged the occupations and considered the Se (Te) atoms in the octahedral (trigonal) symmetry and vice versa (see Supplementary Information Section VII). We found that, at the DFT level, the relaxed 6R structure consisting of alternating 1T-$NbTe_2$-1H-$NbSe_2$ layers is 0.1 eV/Nb atom more stable than the 1H-$NbTe_2$-1T-$NbSe_2$ structure. The solution with disordered ligands (of higher energy) shows a different type of imaginary modes, peaking in this case at the M point [see Fig. 3(d)]. Therefore, this result suggests that ligand disorder decreases the coherence of the $\frac{1}{2}\overline{\Gamma M}$-peaks, thus quenching the formation of a long-range CDW and establishing the short-range charge correlations observed experimentally.

Finally, Figs. 3(e) and 3(f) show the temperature de-

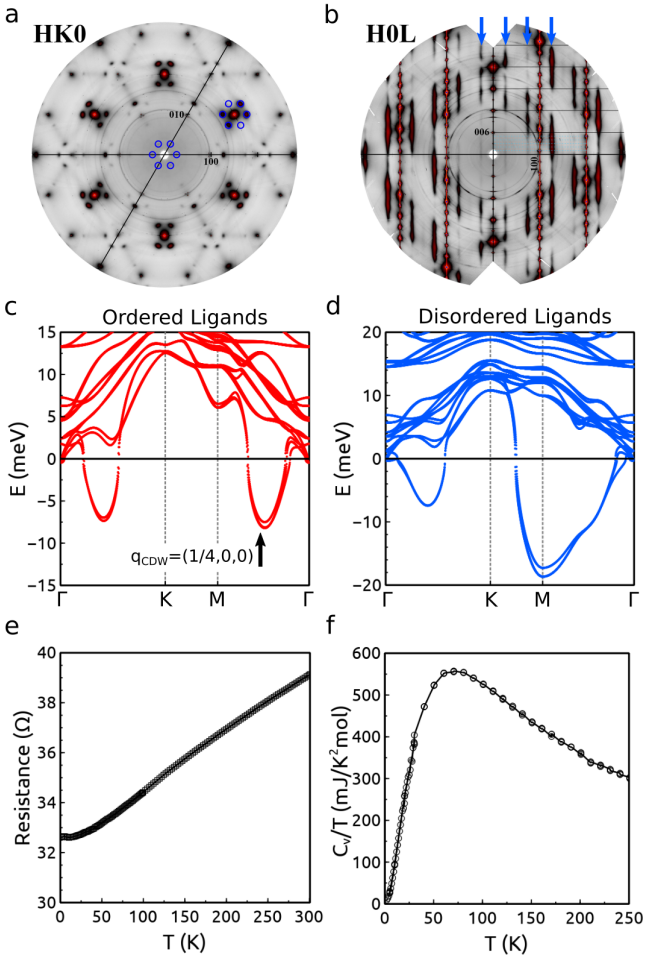

FIG. 3. (a) HK0 and (b) H0L diffuse scattering maps of NbSeTe at 80 K. See Supplementary Information Fig. S6 for the DS at room temperature. Strong DS is observed in the vicinity of the 110 Bragg peak in (a) and as rods along the L-direction in (b), highlighted with blue circles and arrows respectively. (c-d) Harmonic phonon spectra for the structure having $NbSe_2$ ($NbTe_2$) with local 1H (1T) coordination (ordered ligands) and one with different ligands both in 1H and 1T coordination (called disordered ligands, see Supplementary Information Section VII). Two imaginary modes appear to be competing, but triply degenerate. Only the Γ to M mode is seen in our experiments, suggesting that the other one is absent by the competition between possible orders. The disordered ligands plot shows the imaginary modes displaced towards the M point. (e) Temperature dependence of the resistance for the NbTeSe single crystal. (f) Temperature-dependent heat capacity measurement at H =0 T.

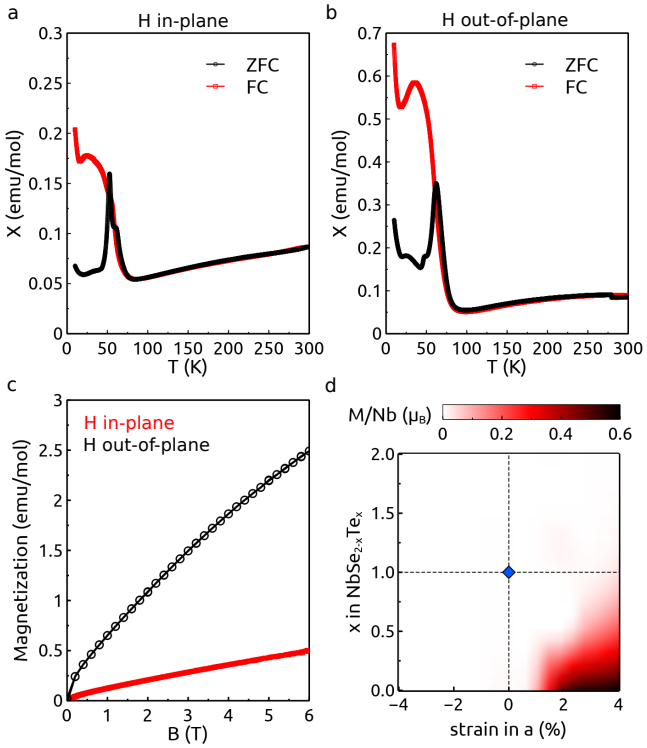

FIG. 4. (a) Temperature dependence of magnetic susceptibility for NbTeSe measured in the zero-field-cooled and a field-cooled condition for an applied magnetic field H= 0.5 T with H$\|ab$-plane and (b) out-of-plane, H$\|c$-axis. (c) Magnetization as a function of magnetic field (M *vs* H) at 10 K temperature for a magnetic field applied parallel and perpendicular to the ab-plane of the single crystal. (d) Calculated magnetic moment color map as a function of Te concentration x in the $Nb_{2-x}Te_x$ system and strain in the in-plane lattice parameter a. Non-zero magnetization in the supercells develops at tensile strains and low Te concentrations.

pendence of the resistance and specific heat of the compound. No phase transition appears to accompany the charge correlations seen in DS experiments. Moreover, the resistance shows no abrupt changes at any temperature that can signal a transition to a long-range order CDW or gap opening. The dependence of the resistance with temperature is roughly linear with a positive slope and flattening at very low temperatures. There is a change in the slope of the specific heat at about 60 K, but no trace of a real phase transition. Besides, we find no signal of superconductivity in any of our measurements down to 2K, in contrast to the 1T-NbSeTe polymorph [33] and the parent compound 2H-$NbSe_2$ [30]. This quenching of the superconducting order in 6R-NbSeTe compared with the 2H-$NbSe_2$ can be understood from a self-doping mechanism caused by the substitution of Se by the less electronegative Te [36]. This produces a shift in the chemical potential of the DOS of Nb atom in the T environment [as shown in Fig. 2(i)], thus leading to a lower DOS at the Fermi level and, hence, obliterating superconductivity. Other factors like ligand disorder could also be related to the quenching, hence further studies are required to elucidate this point.

We now turn our attention to the presence of magnetism in 6R-NbSeTe. Remarkably, the weak charge modulations are accompanied by the emergence of short-range magnetic order below $\sim$ 60 K. Figures 4(a) and

4(b) show the zero field cooled-field cooled (ZFC-FC) magnetic susceptibility curves of NbSeTe collected under a 0.5 T magnetic field [in-plane (a) and out-of-plane (b)]. The susceptibility initially decreases linearly from 300 K, typical of low dimensional systems, before steeply raising below 60 K. The large splitting of the ZFC-FC indicates a strongly inhomogeneous magnetic ground state [51] with an out-of-plane magnetic anisotropy. The inhomogeneous magnetic state is further confirmed by the absence of a λ-like anomaly in heat capacity data and by the absence of magnetoresistance at low temperature. Also, the very small value of the magnetization (on the order of 10^{-3} μ_B/Nb) points to its glassy origin.

The picture that builds up as the ground state in NbSeTe is of an entangled short-ranged charge/spin correlated ground state. To theoretically understand its microscopic origin, we have carried out DFT calculations in the 6R phase of $NbSe_{2-x}Te_x$ at different values of strain that internally build up due to the Se/Te substitution. Figure 4(d) shows the phase diagram describing the evolution of the magnetization as a function of the ligand substitution and strain. From our *ab initio* calculations, we have analyzed various Te concentrations in $NbSe_{2-x}Te_x$ supercells at various degrees of strain. We observe that the system is typically non-magnetic, but in the tensile strain limit of the in-plane lattice parameter a stretched by 2-4% and low Te concentrations ($x < 1.0$), a non-zero magnetization emerges. Given the degree of Se/Te disorder and the observed magnetic glassy behavior with a small value of the total magnetization in our samples, we interpret our experimental data on the basis of Se-rich clusters, where the local strain will produce the short-range magnetic order that gives rise to the small magnetization and ZFC-FC splitting below a certain blocking temperature. Indeed, our approach resembles the used of controlled disorder to tune the interplay between charge order and superconductivity in $NbSe_2$ [52].

From the CDW q-vector we have found in the DS experiments, we have carried out additional calculations in a $4 \times 4 \times 1$ supercell to elucidate if the local-charge modulations could give rise to the emergence of magnetism (see Supplementary Information Fig. S11). Relaxing this structure allows us to visualize in real space the striped nature (with an off-plane modulation) of this CDW (which is a lower-energy state compared to the undistorted structure). The calculations including spin polarization lead to a non-magnetic solution, with the higher moment solutions all higher in energy. Thus, the CDW itself does not bring about the observed magnetic signal. The reduction of the charge correlation length compared with the parent compounds 2H-$NbSe_2$ and 1T-$NbTe_2$ and the emergence of short-range magnetism show parallels to the real space spatial distribution of charge/spin and superconducting domains in superconducting cuprates [53–56].

The question of whether the decoupled 1T-1H heterobilayers and the disordered local moment picture have anything to do with Kondo physics should be addressed, in particular given the resistivity data flattening at low temperatures. From the measurements of the specific heat, we extract a value for the Sommerfeld coefficient of about 5.1 mJ/mol·K^2 while the value coming from our DFT calculations (at the uncorrelated GGA level) is 4.7 mJ/mol·K^2. The good agreement between DFT and the experiment highlights the absence of Kondo physics in this system. Considering the absence of magnetic impurities in the sample (see Supplementary Information Fig. S8), in our view, the magnetism observed here can be better explained by our calculations showing that magnetic moments may arise due to local ligand inhomogeneities and local strains in the system. This point of view is also supported by the absence of flat bands close to the Fermi level observed in the ARPES measurements (Fig. 2) in contrast to the 1T-1H bilayers of TaS_2[21, 57, 58].

In summary, we have presented a new type of naturally occurring $NbSe_2$-$NbTe_2$ TMD heterostructure crystallizing in the rhombohedral 6R phase that features a spatial distribution of short-range charge and spin orders. The combination of experimental data and *ab initio* calculations have demonstrated the c-axis stacking of H and T layers and how chemical disorder drives the presence of magnetism and electronic modulations with propagation vectors differing from the parent compounds. Our work also demonstrates the great versatility of the TMD layered structure to engineer new correlated phases of matter and opens the possibility of studying exotic ground states by means of bulk techniques (diffraction, magnetization,...), not possible for artificially stacked 2D monolayers or MBE grown TMDs.

We thank Fernando de Juan, Eduardo da Silva Neto and Yu He for fruitful discussions and critical reading of the manuscript. This work was supported by the MINECO of Spain, projects PID2021-122609NB-C21 and PID2021-122609NB-C22. S.B-C and A.K thank the MCIN and the European Union Next Generation EU/PRTR-C17.I1, as well as by IKUR Strategy under the collaboration agreement between Ikerbasque Foundation and DIPC on behalf of the Department of Education of the Basque Government. A. O. F. thanks the financial support from the Academy of Finland Project No. 349696. J. P. thanks MECD for the financial support received through the 'Ayudas para contratos predoctorales para la formación de doctores' grant PRE2019-087338. We acknowledge the computational resources provided by the Galician Supercomputing Center (CESGA) and the Aalto Science-IT project. We acknowledge DESY (Hamburg, Germany), a member of the Helmholtz Association HGF, for the provision of experimental facilities. Parts of this research were carried out at PETRA III using beamline P04. Beamtime was allocated for proposal I/II-20191409. The photoemission spectroscopy instrument at beamline P04 was funded by the German Federal Ministry of Education and Research (BMBF) under the framework program ErUM (projects 05KS7FK2, 05K10FK1,

05K12FK1, 05K13FK1, 05K19FK4 with Kiel University; 05KS7WW1, 05K10WW2, and 05FK19WW2 with the University of Würzburg). Sample growth was supported by the German Research Foundation (DFG), project 434434223-SFB 1461. This work has been partly performed in the framework of the nanoscience foundry and fine analysis (NFFA-MUR Italy Progetti Internazionali) facility. We would like to acknowledge the use of Servicio General de Apoyo a la Investigación-SAI, Universidad de Zaragoza, for the specific heat measurements.

III. METHODS

Single crystals of NbSeTe were grown by the standard chemical vapor transport method: A near-stoichiometric mixture of high-purity Nb, Se and Te was placed in a quartz ampoule together with iodine (5 mg/cm^3) as transport agent; the ampoule was sealed and heated in a four-zone furnace under a temperature gradient of 850-765°C for 2 weeks. The formation of polytypes was prevented by quenching of the hot ampoules in water. Typical crystal sizes were about 3×3×0.5 mm^3.

Single crystal diffraction and diffuse scattering were performed at the ID28 beamline at the European Synchrotron Radiation Facility (ESRF) with E_i=17.8 keV and a Dectris PILATUS3 1M X area detector. The CrysAlis software package was used for the orientation matrix refinement. Reciprocal space maps were reconstructed with ID28 software ProjectN and subsequently plotted in Albula.

Soft x-ray ARPES measurements were carried out at the P04 beamline of PETRA III at DESY using the ASPHERE photoelectron spectroscopy endstation and vacuum ultra-violet ARPES at the APE-LE beamline of ELETTRA. The soft X-ray photon energy and total energy resolution used were 432 eV and 80 meV, respectively. The vacuum ultra-violet photon energy and total energy resolution used were 55 eV and 30 meV, respectively. The angular resolutions were better than 0.1 degree.

High resolution STEM imaging has been performed on TitanG2 60-300 electron microscope (FEI), equipped with x-FEG electron source, monochromator and HAADF detector. For STEM imaging the microscope was operated at 300kV at spotzise 9 and monochromator at -100V gun lens excitation below focus. Overview images were acquired in one 1Kx1K scan with 30us dwell time. Images for structure analysis were acquired as a rapid sequence of 100 1K×1K frames with a dwell time of 500ns, which were subsequently aligned and averaged. Projection of the unit cell has been identified and averaged over the image resulting in 126 individual averaged cells in Figure 1. EDX analysis was made on a probe-corrected Spectra 30-300 STEM (ThermoFisher) operated at 300 kV. Atomic resolution EDX maps were acquired with a probe current of 150 pA using Velox, and rapid rastered scanning. The Energy-Dispersive X-Ray (EDX) signal was acquired on a Dual-X system with a total acquisition angle of 1.76 Sr comprising two detectors either side of the sample.

ab initio electronic structure calculations based on Density Functional Theory (DFT) [59] were performed using an all electron full-potential code (WIEN2k [60]). The generalized gradient approximation (GGA)[61] was used as the exchange-correlation term for all of our calculations. The harmonic phonon spectrum of the charge-density wave (CDW) phase of NbSeTe was computed using the Phonopy code [62]. Taking the 6R structure as the unit cell, we have performed calculations of a 4×4 supercell ($6 \times 6 \times 2$ k-mesh). We have used the VASP [63–65] code for this task and for all the structural relaxations with the different geometries analyzed (see Suppl. Information for further details).

[1] Geim, A. K.; Grigorieva, I. V. *Nature* **2013**, *499*, 419–425.

[2] Novoselov, K. S.; Mishchenko, A.; Carvalho, A.; Neto, A. H. C. *Science* **2016**, *353*, aac9439.

[3] Zeng, M.; Xiao, Y.; Liu, J.; Yang, K.; Fu, L. *Chemical Reviews* **2018**, *118*, 6236–6296.

[4] Manzeli, S.; Ovchinnikov, D.; Pasquier, D.; Yazyev, O. V.; Kis, A. *Nature Reviews Materials* **2017**, *2*, 1–15.

[5] Nair, N. L.; Maniv, E.; John, C.; Doyle, S.; Orenstein, J.; Analytis, J. G. *Nature Materials* **2020**, *19*, 153–157.

[6] Takagi, H. et al. *Nature Physics* **2023**, *19*, 961–968.

[7] Wu, S.; Basak, R.; Li, W.; Kim, J.-W.; Ryan, P. J.; Lu, D.; Hashimoto, M.; Nelson, C.; Acevedo-Esteves, R.; Haley, S. C.; Analytis, J. G.; He, Y.; Frano, A.; Birgeneau, R. J. *Phys. Rev. Lett.* **2023**, *131*, 186701.

[8] Yu, Y.; Yang, F.; Lu, X. F.; Yan, Y. J.; Cho, Y.-H.; Ma, L.; Niu, X.; Kim, S.; Son, Y.-W.; Feng, D.; Li, S.; Cheong, S.-W.; Chen, X. H.; Zhang, Y. *Nature Nanotechnology* **2015**, *10*, 270–276.

[9] Ang, R.; Tanaka, Y.; Ieki, E.; Nakayama, K.; Sato, T.; Li, L. J.; Lu, W. J.; Sun, Y. P.; Takahashi, T. *Phys. Rev. Lett.* **2012**, *109*, 176403.

[10] Abramchuk, M.; Jaszewski, S.; Metz, K. R.; Osterhoudt, G. B.; Wang, Y.; Burch, K. S.; Tafti, F. *Advanced Materials* **2018**, *30*, 1801325.

[11] Tartaglia, T. A.; Tang, J. N.; Lado, J. L.; Bahrami, F.; Abramchuk, M.; McCandless, G. T.; Doyle, M. C.; Burch, K. S.; Ran, Y.; Chan, J. Y.; Tafti, F. *Science Advances* **2020**, *6*, eabb9379.

[12] Cole, A.; Streeter, A.; Fumega, A. O.; Yao, X.; Wang, Z.-C.; Feng, E.; Cao, H.; Lado, J. L.; Nagler, S. E.; Tafti, F. *Phys. Rev. Mater.* **2023**, *7*, 064401.

[13] Guo, H.-W.; Hu, Z.; Liu, Z.-B.; Tian, J.-G. *Advanced Functional Materials* **2021**, *31*, 2007810.

[14] Li, H.; Li, Y.; Aljarb, A.; Shi, Y.; Li, L.-J. *Chemical reviews* **2017**, *118*, 6134–6150.

[15] Cao, Y.; Fatemi, V.; Demir, A.; Fang, S.;

Tomarken, S. L.; Luo, J. Y.; Sanchez-Yamagishi, J. D.; Watanabe, K.; Taniguchi, T.; Kaxiras, E.; Ashoori, R. C.; Jarillo-Herrero, P. *Nature* **2018**, *556*, 80–84.
[16] Cao, Y.; Fatemi, V.; Fang, S.; Watanabe, K.; Taniguchi, T.; Kaxiras, E.; Jarillo-Herrero, P. *Nature* **2018**, *556*, 43–50.
[17] Shabani, S.; Halbertal, D.; Wu, W.; Chen, M.; Liu, S.; Hone, J.; Yao, W.; Basov, D. N.; Zhu, X.; Pasupathy, A. N. *Nature Physics* **2021**, *17*, 720–725.
[18] Zeng, Y.; Xia, Z.; Kang, K.; Zhu, J.; Knüppel, P.; Vaswani, C.; Watanabe, K.; Taniguchi, T.; Mak, K. F.; Shan, J. *Nature* **2023**, *622*, 69–73.
[19] Cai, J. et al. *Nature* **2023**, *622*, 63–68.
[20] Kezilebieke, S.; Huda, M. N.; Vaňo, V.; Aapro, M.; Ganguli, S. C.; Silveira, O. J.; Głodzik, S.; Foster, A. S.; Ojanen, T.; Liljeroth, P. *Nature* **2020**, *588*, 424–428.
[21] Vaňo, V.; Amini, M.; Ganguli, S. C.; Chen, G.; Lado, J. L.; Kezilebieke, S.; Liljeroth, P. *Nature* **2021**, *599*, 582–586.
[22] Di Salvo, F.; Bagley, B.; Voorhoeve, J.; Waszczak, J. *Journal of Physics and Chemistry of Solids* **1973**, *34*, 1357–1362.
[23] Wang, Y.; Yao, W.; Xin, Z.; Han, T.; Wang, Z.; Chen, L.; Cai, C.; Li, Y.; Zhang, Y. *Nature communications* **2020**, *11*, 4215.
[24] Ribak, A.; Skiff, R. M.; Mograbi, M.; Rout, P. K.; Fischer, M. H.; Ruhman, J.; Chashka, K.; Dagan, Y.; Kanigel, A. *Science Advances* **2020**, *6*, eaax9480.
[25] Nayak, A. K.; Steinbok, A.; Roet, Y.; Koo, J.; Margalit, G.; Feldman, I.; Almoalem, A.; Kanigel, A.; Fiete, G. A.; Yan, B.; Oreg, Y.; Avraham, N.; Beidenkopf, H. *Nature Physics* **2021**, *17*, 1413–1419.
[26] Achari, A.; Bekaert, J.; Sreepal, V.; Orekhov, A.; Kumaravadivel, P.; Kim, M.; Gauquelin, N.; Balakrishna Pillai, P.; Verbeeck, J.; Peeters, F. M., et al. *Nano Letters* **2022**, *22*, 6268–6275.
[27] Battaglia, C.; Cercellier, H.; Clerc, F.; Despont, L.; Garnier, M. G.; Koitzsch, C.; Aebi, P.; Berger, H.; Forró, L.; Ambrosch-Draxl, C. *Phys. Rev. B* **2005**, *72*, 195114.
[28] Lian, C.-S.; Si, C.; Duan, W. *Nano letters* **2018**, *18*, 2924–2929.
[29] Du, C.-H.; Lin, W. J.; Su, Y.; Tanner, B. K.; Hatton, P. D.; Casa, D.; Keimer, B.; Hill, J. P.; Oglesby, C. S.; Hohl, H. *Journal of Physics: Condensed Matter* **2000**, *12*, 5361.
[30] Borisenko, S. V.; Kordyuk, A. A.; Zabolotnyy, V. B.; Inosov, D. S.; Evtushinsky, D.; Büchner, B.; Yaresko, A. N.; Varykhalov, A.; Follath, R.; Eberhardt, W.; Patthey, L.; Berger, H. *Phys. Rev. Lett.* **2009**, *102*, 166402.
[31] Cossu, F.; Moghaddam, A. G.; Kim, K.; Tahini, H. A.; Di Marco, I.; Yeom, H.-W.; Akbari, A. *Phys. Rev. B* **2018**, *98*, 195419.
[32] Cossu, F.; Palotás, K.; Sarkar, S.; Di Marco, I.; Akbari, A. *NPG Asia Materials* **2020**, *12*, 24.
[33] Yan, D.; Wang, S.; Lin, Y.; Wang, G.; Zeng, Y.; Boubeche, M.; He, Y.; Ma, J.; Wang, Y.; Yao, D.-X., et al. *Journal of Physics: Condensed Matter* **2019**, *32*, 025702.
[34] Luo, H.; Xie, W.; Tao, J.; Inoue, H.; Gyenis, A.; Krizan, J. W.; Yazdani, A.; Zhu, Y.; Cava, R. J. *Proceedings of the National Academy of Sciences* **2015**, *112*, E1174–E1180.
[35] Liu, Y.; Shao, D.-F.; Li, L.; Lu, W.; Zhu, X.; Tong, P.; Xiao, R.; Ling, L.; Xi, C.; Pi, L., et al. *Physical Review B* **2016**, *94*, 045131.
[36] Phillips, J.; Lado, J. L.; Pardo, V.; Fumega, A. O. *arXiv preprint arXiv:2306.12493* **2023**,
[37] Wang, H. et al. *Nature Communications* **2017**, *8*, 394.
[38] Rossnagel, K. *Journal of Physics: Condensed Matter* **2011**, *23*, 213001.
[39] Johannes, M. D.; Mazin, I. I.; Howells, C. A. *Phys. Rev. B* **2006**, *73*, 205102.
[40] Diego, J.; Said, A. H.; Mahatha, S. K.; Bianco, R.; Monacelli, L.; Calandra, M.; Mauri, F.; Rossnagel, K.; Errea, I.; Blanco-Canosa, S. *Nature Communications* **2021**, *12*, 598.
[41] Weber, F.; Hott, R.; Heid, R.; Lev, L. L.; Caputo, M.; Schmitt, T.; Strocov, V. N. *Phys. Rev. B* **2018**, *97*, 235122.
[42] Fumega, A. O.; Diego, J.; Pardo, V.; Blanco-Canosa, S.; Errea, I. *Nano Letters* **2023**, *23*, 1794–1800, PMID: 36825982.
[43] Diego, J. et al. *Phys. Rev. B* **2024**, *109*, 035133.
[44] Weber, F.; Rosenkranz, S.; Castellan, J.-P.; Osborn, R.; Hott, R.; Heid, R.; Bohnen, K.-P.; Egami, T.; Said, A. H.; Reznik, D. *Phys. Rev. Lett.* **2011**, *107*, 107403.
[45] Jang, W.-J.; Sim, J.; Heo, J. E.; Noh, H.; Kim, R.; Chang, S. H.; Jeon, S.; Kim, H. W. *Phys. Rev. B* **2022**, *106*, 125110.
[46] Gerber, S. et al. *Science* **2015**, *350*, 949–952.
[47] Kim, H.-H. et al. *Science* **2018**, *362*, 1040–1044.
[48] Korshunov, A. et al. *Nature Communications* **2023**, *14*, 6646.
[49] Cao, S.; Xu, C.; Fukui, H.; Manjo, T.; Dong, Y.; Shi, M.; Liu, Y.; Cao, C.; Song, Y. *Nature Communications* **2023**, *14*, 7671.
[50] Tan, H.; Yan, B. *Phys. Rev. Lett.* **2023**, *130*, 266402.
[51] Rivadulla, F.; López-Quintela, M. A.; Rivas, J. *Phys. Rev. Lett.* **2004**, *93*, 167206.
[52] Cho, K.; Kończykowski, M.; Teknowijoyo, S.; Tanatar, M. A.; Guss, J.; Gartin, P. B.; Wilde, J. M.; Kreyssig, A.; McQueeney, R. J.; Goldman, A. I.; Mishra, V.; Hirschfeld, P. J.; Prozorov, R. *Nature Communications* **2018**, *9*, 2796.
[53] Alloul, H.; Bobroff, J.; Gabay, M.; Hirschfeld, P. J. *Rev. Mod. Phys.* **2009**, *81*, 45–108.
[54] Suchaneck, A.; Hinkov, V.; Haug, D.; Schulz, L.; Bernhard, C.; Ivanov, A.; Hradil, K.; Lin, C. T.; Bourges, P.; Keimer, B.; Sidis, Y. *Phys. Rev. Lett.* **2010**, *105*, 037207.
[55] Blanco-Canosa, S.; Frano, A.; Loew, T.; Lu, Y.; Porras, J.; Ghiringhelli, G.; Minola, M.; Mazzoli, C.; Braicovich, L.; Schierle, E.; Weschke, E.; Le Tacon, M.; Keimer, B. *Phys. Rev. Lett.* **2013**, *110*, 187001.
[56] Campi, G.; Bianconi, A.; Poccia, N.; Bianconi, G.; Barba, L.; Arrighetti, G.; Innocenti, D.; Karpinski, J.; Zhigadlo, N. D.; Kazakov, S. M.; Burghammer, M.; Zimmermann, M. v.; Sprung, M.; Ricci, A. *Nature* **2015**, *525*, 359–362.
[57] Crippa, L.; Bae, H.; Wunderlich, P.; Mazin, I. I.; Yan, B.; Sangiovanni, G.; Wehling, T.; Valentí, R. *Nature Communications* **2024**, *15*, 1357.
[58] Wan, W.; Harsh, R.; Meninno, A.; Dreher, P.; Sajan, S.; Guo, H.; Errea, I.; de Juan, F.; Ugeda, M. M. *Nature Communications* **2023**, *14*, 7005.
[59] Hohenberg, P.; Kohn, W. *Phys. Rev.* **1964**, *136*, B864–B871.
[60] Blaha, P.; Schwarz, K.; Tran, F.; Laskowski, R.; Madsen, G. K. H.; Marks, L. D. *The Journal of Chemical*

Physics **2020**, *152*, 074101.
[61] Perdew, J. P.; Burke, K.; Ernzerhof, M. *Phys. Rev. Lett.* **1996**, *77*, 3865–3868.
[62] Togo, A.; Tanaka, I. *Scr. Mater.* **2015**, *108*, 1–5.
[63] Kresse, G.; Hafner, J. *Physical review B* **1993**, *47*, 558.
[64] Kresse, G.; Furthmüller, J. *Computational materials science* **1996**, *6*, 15–50.
[65] Kresse, G.; Furthmüller, J. *Physical review B* **1996**, *54*, 11169.